



HAL
open science

Material Modeling via Thermodynamics-Based Artificial Neural Networks

Filippo Masi, Ioannis Stefanou, Paolo Vannucci, Victor Maffi-Berthier

► **To cite this version:**

Filippo Masi, Ioannis Stefanou, Paolo Vannucci, Victor Maffi-Berthier. Material Modeling via Thermodynamics-Based Artificial Neural Networks. Workshop on Joint Structures and Common Foundations of Statistical Physics, Information Geometry and Inference for Learning, SPIGL 2020, 2020, Les Houches, France. pp.308-329, 10.1007/978-3-030-77957-3_16 . hal-03993037

HAL Id: hal-03993037

<https://hal.science/hal-03993037>

Submitted on 12 Mar 2024

HAL is a multi-disciplinary open access archive for the deposit and dissemination of scientific research documents, whether they are published or not. The documents may come from teaching and research institutions in France or abroad, or from public or private research centers.

L'archive ouverte pluridisciplinaire **HAL**, est destinée au dépôt et à la diffusion de documents scientifiques de niveau recherche, publiés ou non, émanant des établissements d'enseignement et de recherche français ou étrangers, des laboratoires publics ou privés.

Material modeling via Thermodynamics-based Artificial Neural Networks

Filippo Masi, Ioannis Stefanou, Paolo Vannucci, and Victor Maffi-Berthier

Abstract Machine Learning methods and, in particular, Artificial Neural Networks (ANNs) have demonstrated promising capabilities in material constitutive modeling. One of the main drawbacks of such approaches is the lack of a rigorous frame based on the laws of physics.

Here we propose a new class of data-driven, physics-based, neural networks for constitutive modeling of strain-rate independent processes at the material point level, which we define as Thermodynamics-based Artificial Neural Networks (TANNs). Relying on automatic differentiation, derivatives of the free-energy, the dissipation rate and their relation with the stress and internal state variables are hardwired in the network.

The proposed network does not have to identify the underlying pattern of thermodynamic laws during training, reducing the need of large data-sets, improving the robustness and the performance of predictions. Finally and more important, the predictions remain thermodynamically consistent, even for unseen data.

TANNs are herein used to model history-dependent materials, with kinematic softening. While the motivating examples considered may be rather simple, we emphasize that the proposed class of ANN can be successfully applied (without any modification) to materials with different or more complex behavior.

Based on these features, TANNs are a starting point for data-driven, physics-based constitutive modeling with neural networks.

Filippo Masi

Institut de Recherche en Génie Civil et Mécanique, UMR 6183, CNRS, Ecole Centrale de Nantes, Université de Nantes, e-mail: filippo.masi@ec-nantes.fr

Ioannis Stefanou

Institut de Recherche en Génie Civil et Mécanique, UMR 6183, CNRS, Ecole Centrale de Nantes, Université de Nantes, e-mail: ioannis.stefanou@ec-nantes.fr

Paolo Vannucci

LMV, UMR 8100, Université de Versailles et Saint-Quentin, e-mail: paolo.vannucci@uvsq.fr

Victor Maffi-Berthier

Ingérop Conseil et Ingénierie, e-mail: victor.maffi-berthier@ingerop.com

1 Introduction

Machine Learning (ML) is increasingly recognized as a promising tool for many scientific branches, from biological to mechanical sciences. At present, several successful applications of ML approaches and, in particular, of Artificial Neural Networks (ANNs) have been implemented for learning representations of material behaviors from data, either originated through experimental tests or detailed micro-mechanical simulations. We refer, without being exhaustive, to the works of Ghaboussi and Sidarta [12], Lefik and Schrefler [33], Jung and Ghaboussi [28], Settgest et al. [45], Liu and Wu [35], Lu et al. [37], Xu et al. [47], Huang et al. [25], Liu and Wu [35], Gajek et al. [10], Gorji et al. [18], Heider et al. [20], Ghavamian and Simone [15], Mozaffar et al. [42], Frankel et al. [9], González et al. [16], Gorji et al. [18].

Further achievements were accomplished in the field of numerical modeling of mechanics. Starting from the so-called autoprogessive trained ANNs proposed by Ghaboussi et al. [14], numerous approaches have been implemented to solve numerical simulations by resorting to ANNs. Neural networks, trained on some data characterizing the response of a given material, can be employed as material subroutines, replacing the standard constitutive equations or algorithms, in numerical simulations [see 33, 28, 34, 45, among others].

In the last two decades, attention has been focused on the implementation of ANN methods for speeding-up the computing time of multiscale analyses for materials with different characteristic lengths (or scales). Indeed, in multiscale simulations, the micro-scale problem has to be solved repeatedly, but with different input parameters, which renders the computing time of such approaches soon prohibitive. Accelerating techniques based on ANNs have been promoted as excellent tools to overcome the aforementioned issues, see e.g. [8, 1, 35, 15, 36].

Nevertheless, constitutive modeling via ANNs has some major issues. For instance, ANNs perform well when evaluated sufficiently close to the training domain. However, the extrapolation capabilities appear limited when predictions are performed for values far beyond the training range. Furthermore, vast amounts of high quality data (e.g. with reduced noise and free of outliers) are generally needed to enable ANNs to identify and learn with high accuracy the constitutive stress-strain response. These issues essentially stems from the lack of a rigorous framework based on the physical laws governing the material systems under investigation. For a trained ANN, nothing guarantees that its predictions will respect the basic principles of thermodynamics, e.g. the first and second laws.

Very recently, a new class of methods, denoted as physics-driven approaches, have received particular attention. We refer, for instance, to Raissi et al. [44] who developed the so-called Physics-Informed Neural Networks (PINNs), for the resolution of partial differential equations by enforcing basic laws of physics, using the *reverse-mode autodiff* technique [2]. In the field of mechanics, we record the works of González et al. [17], Hernández et al. [21] in which, by leveraging the metriplectic structure of dissipative Hamiltonian systems, the behavior of physical systems can be retrieved by ANNs, whose predictions comply with the first and

second principles of thermodynamics.

In the field of mechanics and constitutive material modeling, Kirchdoerfer and Ortiz [30] proposed a new data driven computing approach in which the boundary value problem (BVP), in material numerical simulations, is solved directly from experimental material data (measurements), bypassing the ANN material modeling step [30, 26, 31, 32, 27, 6]. The integration of basic laws of thermodynamics, in the forms of a minimization problem, allows predictions to fulfill physical requirements, such as the thermodynamic consistency.

With the aim of accelerating multiscale simulations, we propose here a new class of Artificial Neural Networks for the material modeling, based on the basic laws of thermodynamics. Our method, which we denote as Thermodynamics-based Artificial Neural Networks (TANNs), assures thermodynamically consistent network's predictions, for data both close to and beyond the training domain. The proposed approach can be advantageous when modeling complex and abstract constitutive behaviors, which are not a priori known. It can be used even if the BVP does not have a unique solution due to important non-linearities and bifurcation phenomena (e.g. loss of uniqueness, strain localization at the length of interest, multiphysics, runaway instabilities etc.). Finally, TANNs are characterized by reduced computing time, differently from other thermodynamics-based approaches [6, 7], which render them an excellent accelerating tool for multiscale simulations.

For the implementation of Artificial Neural Networks and Thermodynamics-based Artificial Neural Networks, we leverage Tensorflow v2.0. Source codes are available at <https://github.com/flpmasi/Thermodynamics-Neural-Networks> [39].

This Chapter is organized as follows. Section 2 presents an overview of ANN methods and their implementation for material modeling, denoted here as standard ANNs. We present in Section 3 the new class of Thermodynamics-based Artificial Neural Networks, as opposed to standard ANN methods, for the constitutive modeling, at the material point level. Finally, Section 4 presents a motivating application of our approach in modeling history-dependent material behaviors with kinematic softening. Extensive comparisons with standard ANNs, which are not based on thermodynamics, are also presented.

2 Artificial Neural Networks for constitutive modeling

Machine Learning is a general term to describe a large spectrum of numerical methods. Some of them offer very rich interpolation spaces, which, in theory, could be used for approximating complicated functions belonging to uncommon spaces. Here we focus on the method of Artificial Neural Networks (ANNs), which is considered to be a sub-class of Machine Learning methods. According to Cybenko [4] and Chen and Chen [3], ANNs have proved to be universal approximators, due to their rich interpolation space.

2.1 Artificial Neural networks

Artificial Neural Networks (ANNs) can be regarded as non-linear operators [24, 11], composed of an assembly of mutually connected processing units–nodes–, which take an input signal \mathcal{I} and return the output \mathcal{O} , namely

$$\mathcal{O} = \text{ANN}@\mathcal{I}. \quad (1)$$

ANNs consist of at least three types of layers: input, output and hidden layers, with equal or different number of nodes. Figure 1 depicts a network composed of three hidden layers, with three nodes each, an input layer with three nodes, and an output layer with one node. When an ANN has two or more hidden layers, it is called a deep neural network [11]. Denoting the input array with $\mathcal{I} = (i_t)$, with $t = 1, 2, \dots, n_I$ (n_I is the number of inputs), and the outputs with $\mathcal{O} = (o_j)$, with $j = 1, 2, \dots, n_O$ (n_O is the number of outputs), the signal flows from layer $(l - 1)$ to layer (l) according to

$$p_k^{(l)} = \mathcal{A}^{(l)} \left(z_k^{(l)} \right), \quad \text{with} \quad z_k^{(l)} = \sum_s^{n_N^{(l-1)}} \left(w_{ks}^{(l)} p_s^{(l-1)} \right) + b_k^{(l)}, \quad (2)$$

where $p_k^{(l)}$ are the outputs of node k , at layer (l) ; $\mathcal{A}^{(l)}$ is the activation function of layer (l) ; $n_N^{(l-1)}$ is the number of neurons in layer $(l - 1)$; $w_{ks}^{(l)}$ are the *weights* between the s -th node in layer $(l - 1)$ and the k -th node in layer (l) ; and $b_k^{(l)}$ are the *biases* of layer (l) .

The weights and biases of interconnections are adjusted, in an iterative procedure [gradient descent algorithm 11], to minimize the error between the benchmark, $\bar{\mathcal{O}}$, and prediction, \mathcal{O} , that is measured by a loss function, \mathcal{L} . In the following, the Mean (over a set of N samples) Absolute Error (MAE) is used as loss function, i.e.,

$$\mathcal{L} = \frac{\sum_{i=1}^N |\bar{\mathcal{O}}_i - \mathcal{O}_i|}{N}, \quad (3)$$

where $i = 1, 2, \dots, N$. The errors related to each node of the output layer are hence back-propagated to the nodes in the hidden layers and used to calculate the gradients of the loss function, namely

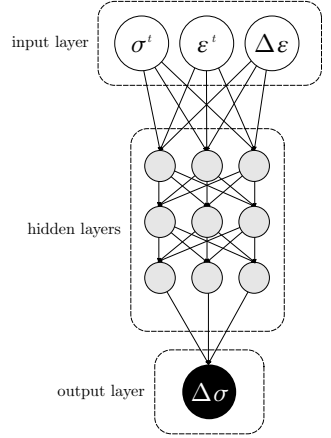
$$\begin{aligned} \frac{\partial \mathcal{L}}{\partial w_{ks}^{(l-m)}} &= \frac{\partial z_k^{(l-m+1)}}{\partial w_{ks}^{(l-m)}} \frac{\partial p_k^{(l-m+1)}}{\partial z_k^{(l-m+1)}} \frac{\partial \mathcal{L}}{\partial p_k^{(l-m+1)}} \\ \frac{\partial \mathcal{L}}{\partial p_k^{(l-m)}} &= \sum_{j=1}^{n_N^{(l-m+1)}} \frac{\partial z_j^{(l-m+1)}}{\partial p_k^{(l-m)}} \frac{\partial p_j^{(l-m+1)}}{\partial z_j^{(l-m+1)}} \frac{\partial \mathcal{L}}{\partial p_j^{(l-m+1)}} \end{aligned} \quad (4)$$

which are then used to update weights and biases, and force the minimization of the loss function values, i.e.

$$w_{ks}^{(l)-\text{new}} := w_{ks}^{(l)} - \epsilon \frac{\partial \mathcal{L}}{\partial w_{ks}^{(l)}}, \quad (5)$$

where ϵ is the so-called learning rate. The weights and biases updating, the so-

Fig. 1 Graph illustration of an ANN structure with three inputs, one output, and three hidden layer with three nodes. In particular, the ANN structure models the incremental stress-strain constitutive response of a material. From the knowledge of the material state at time t , the model predicts the material stress increment, $\Delta\sigma$, corresponding to the given material strain increment, $\Delta\varepsilon$.



called training process, is performed on a subset of the input-output data-set, defined as training set, known from experimental tests or numerical simulations of the phenomenon investigated. The ANN is trained. The training process is stopped as the loss function is below a specific tolerance. Then a test set, a subset of the input-output data-set different to the training set, is used to check the error of the network predictions. Once the ANN is trained, it is used in recall mode to obtain the output of the problem at hand.

Although ANNs have proved to be universal approximators [4, 3], the choice of hyper-parameters, such as the number of neurons, the network topology, the weights, etc. are problem-dependent. The same stands for the activation functions, which may be chosen to have some desirable properties of non-linearity, differentiation, monotonicity, etc. Most of these properties stem from issues related to the gradient descent algorithm and the so-called vanishing gradient problem.

2.2 Material modeling via Artificial Neural networks

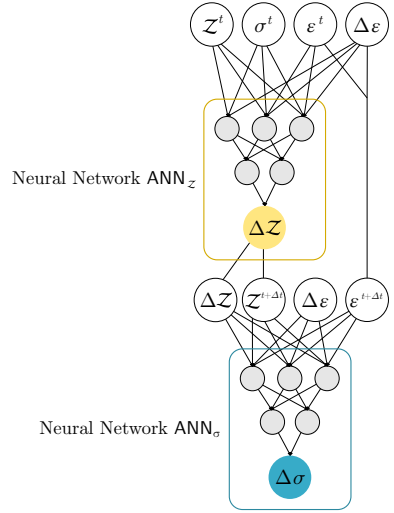
Artificial Neural Networks (ANNs) have demonstrated to be successful in the constitutive modeling of history-dependent materials from model identification based on experiments and detailed numerical simulations. Starting from the seminal work of Ghaboussi et al. [13] and without being exhaustive, we refer to Ghaboussi and Sidarta [12], Lefik and Schrefler [33], Jung and Ghaboussi [28], Settgest et al. [45], Liu and Wu [35], Lu et al. [37], Xu et al. [47], Huang et al. [25], Liu and Wu [35], Gajek et al. [10], Gorji et al. [18], Heider et al. [20], Ghavamian and

Simone [15], Mozaffar et al. [42], Frankel et al. [9], González et al. [16], Gorji et al. [18]. The main idea in these works is to appropriately train ANNs, feeding them with material data, and predict the material response at the material point level. The trained models are then used as material subroutines, replacing the standard constitutive equations or algorithms, in numerical simulations and speed up the otherwise prohibitive computing time of multiscale analyses [1, 38]. This replacement is straightforward and non-intrusive in Finite Element (FE) codes. We record, for instance, the successful embedding of ANNs as material description subroutines in FE codes by Lefik and Schrefler [33], Jung and Ghaboussi [28], Lefik et al. [34], Settigast et al. [45]. Ghavamian and Simone [15] further implemented ANNs in a FE² scheme for accelerating multiscale FE simulations for materials displaying strain softening, with Perzyna viscoplasticity model.

Several ANN models and architectures have been developed to promote the accuracy of the material response predictions. For instance, Figure 1 depicts a variant of the Nested Artificial Neural Networks first proposed by Ghaboussi and Sidarta [12] for the modeling of geo-materials, with history-dependent behavior. Furthermore, we record the works of Heider et al. [20], Mozaffar et al. [42], Gorji et al. [18] who developed ANN models incorporating some knowledge in an informed, guided graph with intermediate history-dependent variables or detecting history-dependent features. We show in Figure 2 the graph of a standard ANN for the modeling of history-dependent material responses. The inputs of the network are the strain increment, $\Delta\varepsilon$, and the material state at time t , characterized by strains, ε^t , stresses, σ^t , and an additional set of variables (e.g., plastic strains, temperature, etc.), denoted here as \mathcal{Z}^t . The model outputs are the additional variables increments (e.g. the plastic strain or temperature increment), $\Delta\mathcal{Z}$, and the stress increments, $\Delta\sigma$, computed via two distinct standard ANNs: $\text{sANN}_{\mathcal{Z}}$ and sANN_{σ} , respectively. In an early work of the authors [40], the foregoing model was successfully used to model von Mises plasticity with kinematic hardening and softening. Nevertheless, several issues afflicting the model accuracy were found. The reason lies in the lack of a rigorous framework based on the laws of physics for standard ANNs, see e.g. [44, 40]. A large number of quality and error-free data is usually needed to enable standard ANNs to identify and learn the underlying thermodynamic laws (although without any guarantee that the predictions will be thermodynamically consistent).

The seminal work of Raissi et al. [44] showed the possibility of adding physical constraints within the architecture of Artificial Neural Networks, by taking advantage of the *reverse-mode autodiff* [2] in the numerical computation of the derivatives of an ANN with respect to its inputs. The new class of physics-based ANNs, denoted as Physics-Informed Artificial Neural Networks (PINNs), demonstrated its superiority with respect to standard ANNs [44]. Inspired by the aforementioned PINNs, Xu et al. [47] developed Symmetric Positive Definite Neural Networks (SPD-NNs) for modeling constitutive relationships by assuring symmetric positive definite stiffness matrices.

Fig. 2 Graph of an informed ANN for the modeling of history-dependent material responses. The inputs of the network are the strain increment, $\Delta\varepsilon$, and the material state at time t , characterized by strains, ε^t , stresses, σ^t , and an additional set of variables, Z^t . The model outputs are the additional variables increments (e.g. the plastic strain or temperature increment), ΔZ , and the stress increments, $\Delta\sigma$, computed via two distinct standard ANNs: sANN $_Z$ and sANN $_\sigma$, respectively



3 Thermodynamics-based Artificial Neural networks

Inspired by the work of Raissi et al. [44], we propose a new class of neural networks based on the laws of thermodynamics, which we denote as Thermodynamics-based Artificial Neural Networks (TANNs). This is accomplished by hardwiring the first and second principle of thermodynamics in the architecture of the network. In comparison with standard ANNs, two additional scalar functions need to be identified in the training data-set. These are the free-energy and the mechanical dissipation rate. However, these quantities are easily accessible in micromechanical simulations [e.g. 8, 43, 46, 29] and can also be obtained experimentally in some cases.

The theoretical framework of our model is presented in paragraph 3.1 and the architecture of TANNs is further detailed in paragraph 3.2.

3.1 Thermodynamics principles and theoretical framework

Let us consider an isothermal constitutive stress-strain response. The (local) power balance equation of energy can be expressed as

$$\dot{F} = W - D, \quad (6)$$

where $W = \sigma \cdot \dot{\varepsilon}$ is the mechanical rate of work, with σ being the Cauchy stress tensor, ε and $\dot{\varepsilon}$ the infinitesimal strain tensor and its rate of change, and " \cdot " denoting the contraction of adjacent indices; F and \dot{F} are the Helmholtz free energy potential and its rate of change; and D is the rate of the mechanical dissipation.

From the second principle of thermodynamics, the rate of the mechanical dissipation must be non-negative,

$$D \geq 0. \quad (7)$$

Furthermore, let us consider strain-rate independent constitutive material responses with the following form of the Helmholtz free energy,

$$F := \tilde{F}(\boldsymbol{\varepsilon}, \mathcal{Z}), \quad (8)$$

and dissipation rate,

$$D := \tilde{D}(\boldsymbol{\varepsilon}, \mathcal{Z}, \dot{\mathcal{Z}}), \quad (9)$$

being a first-order homogeneous function of $\dot{\mathcal{Z}}$, where $\mathcal{Z} = (\zeta_1, \dots, \zeta_N)$ denotes a set of N (additional) internal state variables, ζ_i , $i = 1, \dots, N$. We define here (thermodynamic) state variables those macroscopic quantities characterizing the state of a system, see e.g. [41]. The physical representation of ζ_i is not *a priori* prescribed. For instance, in the case of isotropic damage, ζ is a scalar; for anisotropic damage, a tensor; in the case of elasto-plasticity, a second order tensor, etc. We emphasize that identification of the internal variables set may be not trivial for systems with increasing complexity. As proposed in [6], internal variables can be interpreted as history variables, such as the strain and stress at precedent times. This renders the formalism here adopted general and flexible, depending on the applications.

By time differentiating the energy potential, we obtain

$$\dot{F} = \frac{\partial F}{\partial \boldsymbol{\varepsilon}} \cdot \dot{\boldsymbol{\varepsilon}} + \sum_{i=1}^N \frac{\partial F}{\partial \zeta_i} \cdot \dot{\zeta}_i, \quad (10)$$

which, after substitution in Eq. (6), leads to

$$\left(\frac{\partial F}{\partial \boldsymbol{\varepsilon}} - \boldsymbol{\sigma} \right) \cdot \dot{\boldsymbol{\varepsilon}} - \left(\sum_{i=1}^N \frac{\partial F}{\partial \zeta_i} \cdot \dot{\zeta}_i + D \right) = 0. \quad (11)$$

From the arbitrariness of $\dot{\boldsymbol{\varepsilon}}$ and $\dot{\zeta}_i$, we obtain the following relations

$$\boldsymbol{\sigma} = \frac{\partial F}{\partial \boldsymbol{\varepsilon}}, \quad (12a)$$

$$D = - \sum_{i=1}^N \frac{\partial F}{\partial \zeta_i} \cdot \dot{\zeta}_i. \quad (12b)$$

3.2 Architecture of TANNs

By exploiting the theoretical background presented above, Thermodynamics-based Artificial Neural Networks are ANNs which respect, by definition, the thermodynamic principles, holding true for any class of material. In this framework, TANNs possess the special feature that the entire constitutive response of a material can be derived from definition of only two (pseudo-) potential functions: an energy function and a dissipation function [23]. TANNs are fed with thermodynamics "information", namely Eq.s (12a) and (12b), by relying on the automatic differentiation technique [2] to differentiate neural networks outputs with respect to their inputs. This strategy allows to construct a general framework of neural networks material models which, in principle, can be exploited to predict the behavior of any material and assure that the predictions of TANNs will be thermodynamically consistent even for inputs that exceed the training range of data. Herein, we only focus on strain-rate independent processes. Nevertheless, our approach can be extended, following the developments in [22], to materials showing viscosity and strain-rate dependency.

The model relies on an incremental formulation and can be used in existing Finite Element formulations (among others), see e.g. [33]. Figure 3 illustrates the scheme of TANNs. The model inputs are the strain increment, the previous material state at time t , which is identified herein through the material stress, σ^t , and the internal state variables, ζ_i^t , namely $\mathcal{I} = (\varepsilon^t, \Delta\varepsilon, \sigma^t, \mathcal{Z}^t)$. The *primary* outputs are the internal variables increment, $\Delta\mathcal{Z}$, and the energy potential at time $t + \Delta t$, $F^{t+\Delta t}$. In particular, the increment of the internal variables are predicted by a sub-ANNs,

$$\Delta\mathcal{Z} = \text{ANN}_{\mathcal{Z}} @ \{\varepsilon^t, \Delta\varepsilon^t, \sigma^t, \mathcal{Z}^t\}. \quad (13)$$

A second sub-ANN is used to predict the energy potential, i.e.,

$$F^{t+\Delta t} = \text{ANN}_F @ \{\varepsilon^{t+\Delta t}, \mathcal{Z}^{t+\Delta t}\}. \quad (14)$$

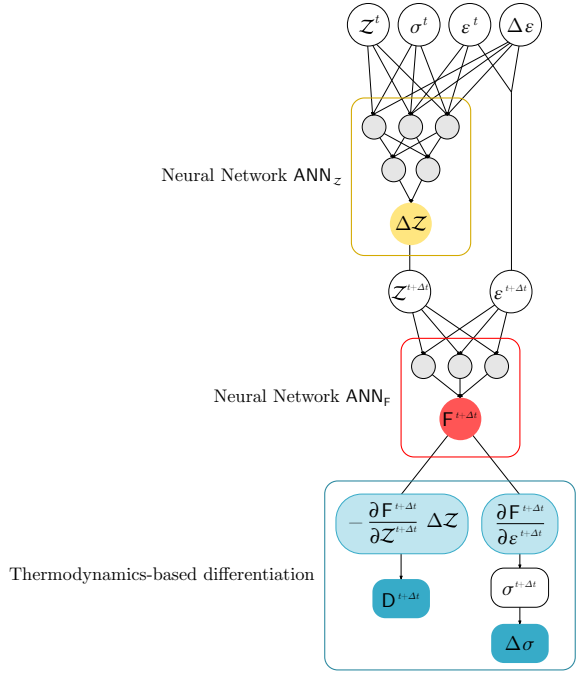
Then, *secondary* outputs—that is, outputs computed by differentiation of the neural network with respect to the inputs—are computed: the stress increment, $\Delta\sigma$, and the dissipation rate, $D^{t+\Delta t}$, i.e., $\nabla_{\mathcal{I}}\mathcal{O} = (\Delta\sigma, D^{t+\Delta t})$. In particular, the stress increment is computed by subtraction of the differential Eq. (12a) and the stress at time t , i.e.,

$$\Delta\sigma = \frac{\partial F^{t+\Delta t}}{\partial \varepsilon^{t+\Delta t}} - \sigma^t. \quad (15)$$

While, the dissipation rate is computed using Eq. (12b), by approximating the rate of the internal variables as $\dot{\mathcal{Z}}^{t+1} \approx \frac{\Delta\mathcal{Z}}{\Delta t}$.

Fig. 3 Graph of Thermodynamics-based Artificial Neural Networks for the isothermal constitutive modeling of strain-rate independent materials. The model involves the following steps:

- (1) prediction of the kinematic variables $\Delta Z = \text{ANN}_Z @ (\varepsilon^{t+\Delta t}, \Delta \varepsilon, \sigma^t, Z^t)$;
- (2) computation of the updated kinematic variables rates, $\dot{Z}^{t+1} \approx \Delta Z / \Delta t$, and the updated kinematic variables, $Z^{t+1} := Z^t + \Delta Z^t$;
- (3) prediction of the updated energy potential $F^{t+\Delta t} = \text{ANN}_F @ \{\varepsilon^{t+\Delta t}, Z^{t+\Delta t}\}$;
- (4) computation of the updated dissipation rate using Eq. (12b);
- (5) computation of the stress increment, Eq. (12a), $\Delta \sigma = \partial F^{t+\Delta t} / \partial \varepsilon^{t+\Delta t} - \sigma^t$.



4 Application to history-dependent materials with softening

Relying on the aforementioned architecture of TANNs, we investigate their ability in modeling the response of history-dependent materials. In particular, we use TANNs in modeling 1D elasto-plastic materials with kinematic softening. While the motivating example we consider may be rather simple, we emphasize that the proposed class of ANN can be successfully applied (without any modification) to materials with different or more complex behavior, see [40].

4.1 Material model and data

The elasto-plastic 1D model with kinematic softening–1D spring-slider [23], see Figure 4–is characterized by the following expressions for the Helmholtz free-energy potential, dissipation rate, and yield function:

$$F = \frac{E}{2} (\varepsilon - \varepsilon^p)^2 + \frac{H}{2} (\varepsilon^p)^2, \quad D = k |\dot{\varepsilon}^p|,$$

and $y = \frac{|\sigma - H\varepsilon^p|}{k} - 1 \leq 0,$

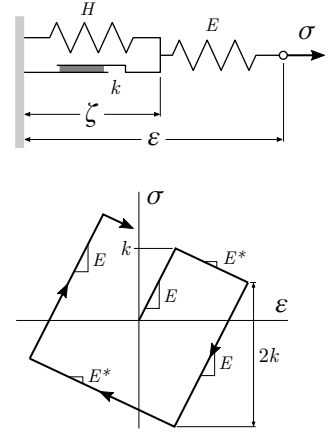
where ε is the total strain; ε^P the plastic strain; σ the Cauchy stress; E the Young modulus; H the kinematic softening parameter; and k the yield strength (slider threshold). The incremental material response is given by

$$\dot{\sigma} = \begin{cases} E\dot{\varepsilon} & \text{when } y < 0, \\ E^*\dot{\varepsilon} & \text{when } y = 0; \end{cases} \quad \dot{\varepsilon}^P = \begin{cases} 0 & \text{when } y < 0, \\ \frac{E^*}{H}\dot{\varepsilon} & \text{when } y = 0; \end{cases} \quad (16)$$

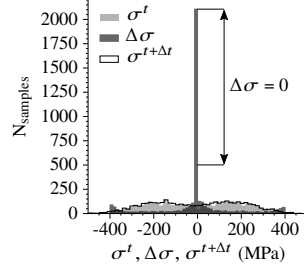
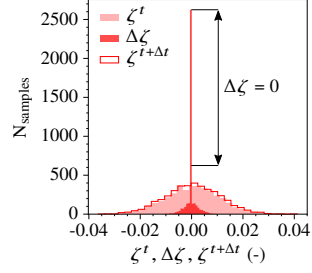
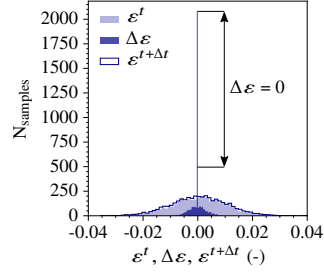
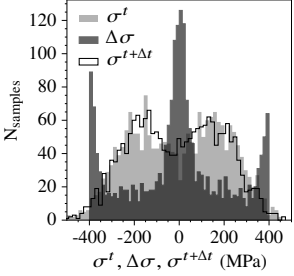
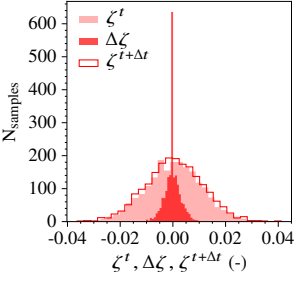
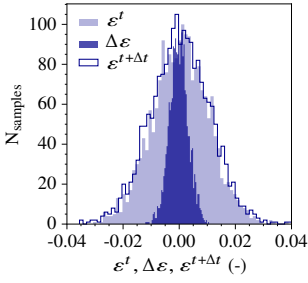
with $E^* = EH/(E + H)$.

As it follows, we consider the following material parameters: $E = 200$ GPa, $k = 200$ MPa, and $H = -100$ MPa. Furthermore, we select the internal variable ζ —see Eq.s (8) and (8)—such that they coincide with the plastic deformation, i.e., $\zeta = \varepsilon^P$. We emphasize that our approach is general and not limited to this kind of state variables.

Fig. 4 Schematic representation of the spring-slider model with kinematic softening (top) and cyclic stress-strain behavior (bottom).



Data are generated by identifying random states for the material at time t . Random strain increments $\dot{\varepsilon}$ are then applied, assuming constant and unitary time increment $\Delta t = 1$ ($\dot{\varepsilon} = \Delta\varepsilon$). The material state at time $t + \Delta t$ is then obtained by numerical integration of the incremental constitutive relations (16). In particular, 2000 data (random increments at random states) are generated. Additionally, an artificial subset of data is considered and constructed assuming $\Delta\varepsilon = 0$ for the initial random states. Such an artificial data-set is added to the generated set of data, in order to facilitate the network to understand that to zero increments of strain correspond zero increments of stress and plastic strain. Figure 5 shows the sampling for total strain, internal variable, and stress. We present in Table 1 the mean (μ), standard deviation (st), and maximum values (max) of the data-set.



(a) 2000 random increments at random states

(b) addition of an artificial subset of data, constructed for $\Delta\varepsilon = 0$

Fig. 5: Sampling of the material data: total strains ε^t , $\Delta\varepsilon$, $\varepsilon^{t+\Delta t}$ (top), plastic strains ζ^t , $\Delta\zeta$, $\zeta^{t+\Delta t}$ (center), and stresses σ^t , $\Delta\sigma$, $\sigma^{t+\Delta t}$ (bottom). 2000 random increments are applied to random states (a), then an artificial subset of data is added considering $\Delta\varepsilon = 0$ for the initial random states (b).

4.2 Training

Training is performed with 50 % of the generated data. A validation set consisting of 25 % of the generated data is used to avoid over-fitting. We take advantage of the technique of *early-stopping*—that is, training is stopped as the error of a validation set starts to increase while the learning error still decreases [11]. Finally, a test set (25 % of the generated data) is used to evaluate the network predictions, once training is accomplished.

The hyper-parameters characterizing the network (i.e., number of hidden layers,

Table 1: Mean (μ), standard deviation (st), and maximum values (max) of the training data-sets.

data		μ	st	max
ε^t	(-)	5×10^{-4}	0.010	0.038
$\Delta\varepsilon$	(-)	1×10^{-4}	0.003	0.040
ζ^t	(-)	5×10^{-4}	0.010	0.040
$\Delta\zeta$	(-)	1×10^{-4}	0.003	0.001
σ_i^t	(MPa)	3.724	208.6	458.8
$\Delta\sigma_i$	(MPa)	-7.745	217.6	400.0
$F^{t+\Delta t}$	(N-mm)	-0.500	0.853	0.105
$D^{t+\Delta t}$	(N-mm/s)	0.384	0.416	2.333

neurons, activation functions, etc.) are selected to give the best predictions, while requiring minimum number of hidden layers and nodes per layer. This is accomplished by comparing the learning error on the set of test patterns, per each trial choice of the hyper-parameters.

Adam optimizer with Nesterov’s acceleration gradient [5] is selected and a batch size of 10 samples is used. We use the Mean Absolute Error (MAE) as loss functions for each output in order to assure the same precision between data of low and high numerical values (cf. Mean Square Error). Regularized weights are used to have consistent order of magnitude of different quantities involved in the loss functions. The architecture of TANNs, as presented in paragraph 3.2 consists of two sub-ANNs. The former, ANN_Z, is composed of four input nodes, one hidden layer with 6 neurons and leaky ReLU activation function, and output node for the predictions of $\Delta\zeta$. The latter sub-network, ANN_F, has two input nodes, one hidden layer with 9 neurons and a modified version of ELU as activation function,

$$\mathcal{A}(z_k) = \begin{cases} z_k^2 & \text{if } z_k > 0, \\ \exp(z_k) - 1 & \text{else,} \end{cases}$$

output node to predict $F^{t+\Delta t}$. The modified ELU activation function is used to avoid the so-called second-order vanishing gradients issue, see [40, 38] for more. The output layers for both sub-networks have linear activation function and biases set to zero. The corresponding number of degrees of freedom, i.e., the number of the hyper-parameters, is 72. Higher number of hidden layers could be used as well, but this is out of the scope of our investigations. Figure 6 displays the loss functions of each output as the training is performed, i.e., in number of epochs. The early stopping rule assures convergence with MAEs of the same order of magnitude for the 4 outputs, $\Delta\zeta$, $F^{t+\Delta t}$, $\Delta\sigma$, and $D^{t+\Delta t}$.

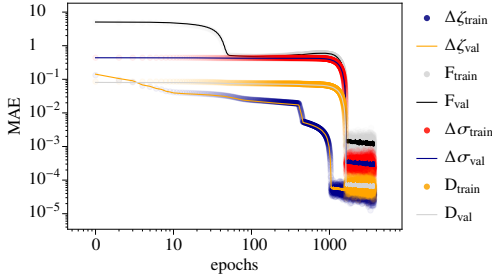


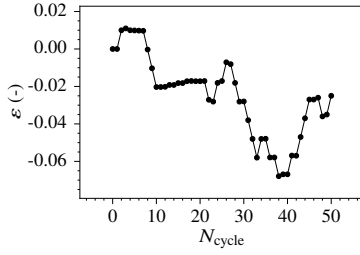
Fig. 6: Errors in terms of the adimensional Mean Absolute Error (MAE) of the predictions of TANN (loss functions), as the training is being performed, evaluated with respect to the training (train) and validation (val) sets. Weights and biases update are computed only on the training set.

4.3 Predictions in recall mode

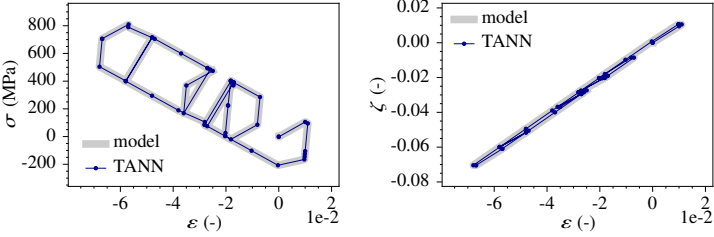
Once the neural network has been trained, we use it in *recall mode* to predict the stress increment for a given strain, strain increment, and possibly other variables, and we compare the predictions with the corresponding targets. The results of the numerical integration scheme—Eq. (16)—are here considered as the exact solution of the material response. In particular, starting from an initial configuration, we make cyclic (or random) increments of the strain, $\Delta\varepsilon$. TANNs hence predict the corresponding increments, $\{\Delta\zeta, \Delta\sigma\}$, which will be transformed into the inputs in the successive call, as well as the energy and dissipation rates, $\{F^{t+\Delta t}, D^{t+\Delta t}\}$. This procedure is applied recursively. The neural network is so self-fed. Figure 7 illustrate the predictions of TANNs for random loading paths with strain increments varying from 10^{-5} and 0.01.

TANNs are found to successfully predict all quantities of interest. Moreover, and most important, the architecture and the training of the network allows to obtain thermodynamically consistent results. The first law of thermodynamics is automatically satisfied as a result of the structure of TANNs and the predicted dissipation rate is always positive. Indeed, even if the second principle of thermodynamics is not explicitly assured by the TANNs architecture, the fact that the training has been performed with consistent material data (i.e., positive dissipation rate) results automatically in the fulfillment of the second principle.

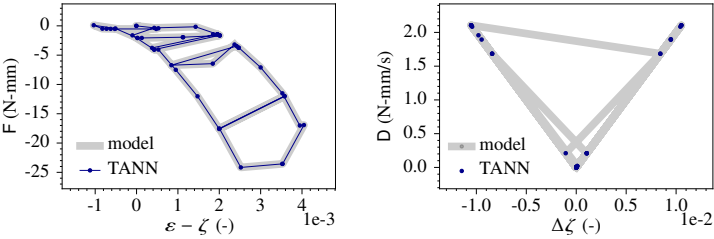
It worth noticing that the random loading path consists of values of strain increments beyond the training range (see Table 1). However, TANNs predictions are extremely accurate. Indeed, the thermodynamics framework renders the generalization capability of TANN (i.e., the ability to make predictions for loading paths different from those used in the training operation) remarkably good. This is usually not observed in standard ANNs as extensively discussed by Lefik and Schrefler [33]. We investigate more in detail the generalization capabilities of our model with respect to standard ANNs, in the next paragraph.



(a) strain increment: $\Delta \varepsilon = 10^{-5}$



(b) strain increment: $\Delta \varepsilon = 10^{-3}$



(c) strain increment: $\Delta \varepsilon = 10^{-2}$

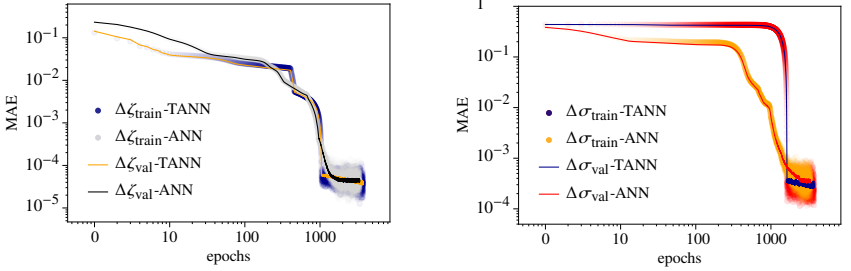
Fig. 7: Predictions of TANNs for a random loading path with strain increments varying from 10^{-5} and 0.01 (beyond the training range, see Table 1): (a) loading path, (b) stress and plastic strain, (c) energy potential and dissipation rate.

4.4 TANNs versus standard ANNs

We compare herein the performance and generalization ability of TANNs with respect to standard ANNs for constitutive modeling [13, 33]. In particular, we select the ANN architecture depicted in Figure 2. The hyper-parameters are selected to give the best performance while assuring the same amount of degrees of freedom, hyper-parameters, with respect to TANNs. Both sub-networks, sANN $_{\zeta}$ and sANN $_{\sigma}$, consist of one hidden layer, with 6 neurons each and leaky ReLU activation function. As for TANNs, the output layers have linear activation function and zero bias. Training is performed on the same set of samples that are used for the thermodynamics-based

network. Figure 8 displays the error of the predictions of standard ANNs, as training is performed, and compares it with TANNs.

It is worth emphasizing that both ANNs and TANNs are dependent on the choice of the user, concerning, for instance, the number of hyper-parameters. Moreover, the actual configurations of both networks may benefit of alternatives/extensions, such as Recurrent Neural Networks. Nevertheless, the following comparisons show the added value of our approach compared to standard ones that do not explicitly contain physics.



(a) Mean Absolute Error (MAE) of $\Delta\zeta$ predictions

(b) Mean Absolute Error (MAE) of $\Delta\sigma$ predictions

Fig. 8: Training of ANNs compared with TANNs evaluated with respect to the training (train) and validation (val) sets.

Once both networks have been trained, we compare the predictions of TANNs and standard ANNs, for a cycling loading path $\Delta\epsilon^t = \Delta\epsilon \operatorname{sgn}(\cos \frac{t\pi}{2N})$ –with $\Delta\epsilon \in (10^{-5}, 1)$. The results are presented in Figure 9, in terms of stress and plastic strain increments.

TANNs are clearly superior in terms of (a) accuracy of the prediction and (b) generalization with respect to the inputs. Moreover, standard ANNs predictions do not fulfill the principles of thermodynamics, even though the training of the network has been performed on consistent material data. This is clearly shown by computing from the predictions of ANNs the increment of the Helmholtz free-energy and dissipation rate using the corresponding definitions, Eq. (4.1). Figure 10 displays the comparison in terms of energy potential, F , and dissipation rate, D . The predictions of the standard ANNs clearly do not respect the thermodynamics principles (both the first and second laws).

We emphasize that even for relatively large and far beyond the training range strain increments, the predictions of TANNs are extremely accurate thanks to their thermodynamic basis. Moreover, TANNs successfully learn the Jacobian, i.e. the elasto-plastic matrix $\frac{\partial\Delta\sigma}{\partial\Delta\epsilon}$ [see 19]. The Jacobian is computed for both networks, standard ANNs and TANNs, as the derivative of the stress increment ($\Delta\sigma$, output) with respect to the strain increment ($\Delta\epsilon$, input). Figure 11 shows the Jacobian and the comparison with the predictions of TANNs and standard ANNs. The excellence

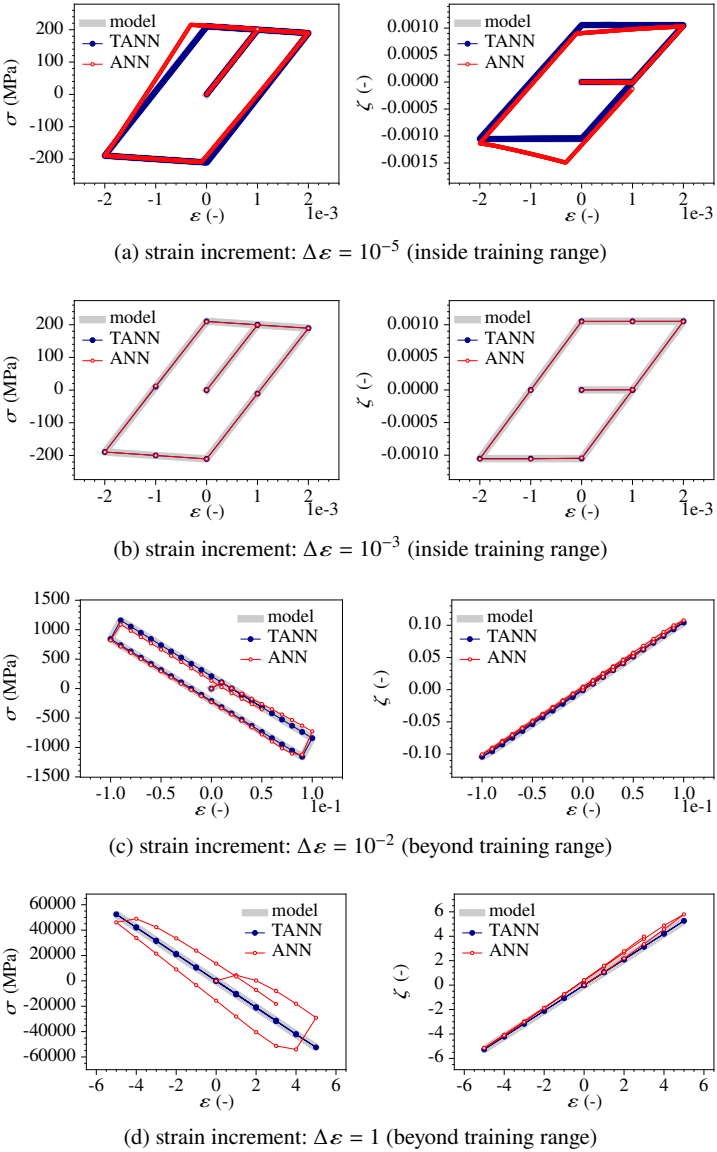


Fig. 9: Predictions of TANNs and standard ANNs for a cyclic loading path, with different strain increments (a-d), in terms of stresses (left column) and plastic strain (right column).

of TANNs is clear: the predictions of the Jacobian are in very good agreement with the reference values (with accuracy between 99.0% and 99.99% for all considered

data-sets). This is not true for standard ANNs, especially for very small and large strain increments.

As a result, TANNs are found to be an excellent candidate for such a substitution, allowing to foresee their application to efficiently speed-up multiscale analyses and FE simulations.

It is worth noticing that increasing the size of the training data-sets and/or the number of layers and neurons could improve the accuracy of standard ANNs. However, there will not be guarantee that the predictions would be thermodynamically consistent. Thermodynamics-based Neural Networks excel over physics-unaware ANNs.

5 Conclusions

A new class of artificial neural networks models to replace constitutive laws and predict the material response at the material point level was proposed. The two basic laws of thermodynamics were directly encoded in the architecture of the model, which we refer to as Thermodynamics-based Neural Networks (TANNs).

TANNs, relying on an incremental formulation and on a theoretical framework of thermodynamics, posses the special feature that the entire constitutive response of a material can be derived from definition of only two scalar functions: the free-energy and the dissipation rate. This assures thermodynamically consistent predictions for data both close to and beyond the training domain. Differently from the standard ANN approaches, TANN does not have to identify, through learning, the underlying thermodynamic laws. Indeed, predictions of standard ANNs may be thermodynamically inconsistent, even though the training of the network has been performed on consistent material data.

For the cases here investigated, TANNs are found to be characterized by high accuracy of the predictions, higher than those of standard approaches. The integration of thermodynamic principles inside the network renders TANN's ability of generalization (i.e., make predictions for loading paths different from those used in the training operation) remarkably good. Consequently, TANNs are excellent candidates for replacing, in future applications, constitutive calculations at Finite Element incremental formulations. Moreover, thanks to the implementation of the free-energy in the network predictions and its thermodynamical relation with the stresses, the Jacobian at the material point level is excellently predicted, even for increments far outside the training data-set range. As a result quadratic convergence in implicit formulations can be preserved, reducing the calculation cost.

Whilst the motivating example to a 1D elasto-plastic material with kinematic softening is easier than real, complex 3D materias, further extensions of TANNs to a wider range of applications are straightforward [see e.g. 40], as the thermodynamics principles hold true for any known class of material, at any length (micro- and macro-scale).

Acknowledgements The author I.S. would like to acknowledge the support of the European Research Council (ERC) under the European Union Horizon 2020 research and innovation program (Grant agreement ID 757848 CoQuake).

References

- [1] M. Alber, A. B. Tepole, W. Cannon, S. De, S. Dura-Bernal, K. Garikipati, G. Karniadakis, W. W. Lytton, P. Perdikaris, L. Petzold, et al. Multiscale modeling meets machine learning: What can we learn? *arXiv preprint arXiv:1911.11958*, 2019.
- [2] A. G. Baydin, B. A. Pearlmutter, A. A. Radul, and J. M. Siskind. Automatic differentiation in machine learning: a survey. *The Journal of Machine Learning Research*, 18(1):5595–5637, 2017.
- [3] T. Chen and H. Chen. Universal approximation to nonlinear operators by neural networks with arbitrary activation functions and its application to dynamical systems. *IEEE Transactions on Neural Networks*, 6(4):911–917, 1995.
- [4] G. Cybenko. Approximation by superpositions of a sigmoidal function. *Mathematics of control, signals and systems*, 2(4):303–314, 1989.
- [5] T. Dozat. Incorporating Nesterov momentum into Adam. 2016.
- [6] R. Eggersmann, T. Kirchdoerfer, S. Reese, L. Stainier, and M. Ortiz. Model-free data-driven inelasticity. *Computer Methods in Applied Mechanics and Engineering*, 350:81–99, 2019.
- [7] R. Eggersmann, L. Stainier, M. Ortiz, and S. Reese. Model-free data-driven computational mechanics enhanced by tensor voting. *arXiv preprint arXiv:2004.02503*, 2020.
- [8] F. Feyel. A multilevel finite element method (FE2) to describe the response of highly non-linear structures using generalized continua. *Computer Methods in Applied Mechanics and Engineering*, 192(28-30):3233–3244, 2003. ISSN 00457825. doi: 10.1016/S0045-7825(03)00348-7.
- [9] A. L. Frankel, R. E. Jones, C. Alleman, and J. A. Templeton. Predicting the mechanical response of oligocrystals with deep learning. *Computational Materials Science*, 169:109099, 2019.
- [10] S. Gajek, M. Schneider, and T. Böhlke. On the micromechanics of deep material networks. *Journal of the Mechanics and Physics of Solids*, page 103984, 2020.
- [11] A. Géron. *Hands-On Machine Learning with Scikit-Learn, Keras, and TensorFlow: Concepts, Tools, and Techniques to Build Intelligent Systems*. O’Reilly Media, 2019.
- [12] J. Ghaboussi and D. Sidarta. New nested adaptive neural networks (NANN) for constitutive modeling. *Computers and Geotechnics*, 22(1):29–52, 1998.
- [13] J. Ghaboussi, J. H. Garrett, and X. Wu. Knowledge-based modeling of material behavior with neural networks. *Journal of Engineering Mechanics*, 117(1): 132–153, 1991. doi: 10.1061/(ASCE)0733-9399(1991)117:1(132).

- [14] J. Ghaboussi, D. A. Pecknold, M. Zhang, and R. M. Haj-Ali. Autoprogressive training of neural network constitutive models. *International Journal for Numerical Methods in Engineering*, 42(1):105–126, 1998.
- [15] F. Ghavamian and A. Simone. Accelerating multiscale finite element simulations of history-dependent materials using a recurrent neural network. *Computer Methods in Applied Mechanics and Engineering*, 357:112594, 2019.
- [16] D. González, F. Chinesta, and E. Cueto. Learning corrections for hyperelastic models from data. *Frontiers in Materials*, 6:14, 2019.
- [17] D. González, F. Chinesta, and E. Cueto. Learning non-markovian physics from data. *Journal of Computational Physics*, 428:109982, 2020.
- [18] M. B. Gorji, M. Mozaffar, J. N. Heidenreich, J. Cao, and D. Mohr. On the potential of recurrent neural networks for modeling path dependent plasticity. *Journal of the Mechanics and Physics of Solids*, page 103972, 2020.
- [19] Y. Hashash, S. Jung, and J. Ghaboussi. Numerical implementation of a neural network based material model in finite element analysis. *International Journal for numerical methods in engineering*, 59(7):989–1005, 2004.
- [20] Y. Heider, K. Wang, and W. Sun. SO(3)-invariance of informed-graph-based deep neural network for anisotropic elastoplastic materials. *Computer Methods in Applied Mechanics and Engineering*, 363:112875, 2020. ISSN 0045-7825. doi: <https://doi.org/10.1016/j.cma.2020.112875>.
- [21] Q. Hernández, A. Badías, D. González, F. Chinesta, and E. Cueto. Structure-preserving neural networks. *Journal of Computational Physics*, page 109950, 2020.
- [22] G. Houslsby and A. Puzrin. A thermomechanical framework for constitutive models for rate-independent dissipative materials. *International journal of Plasticity*, 16(9):1017–1047, 2000.
- [23] G. T. Houslsby and A. M. Puzrin. *Principles of hyperplasticity: an approach to plasticity theory based on thermodynamic principles*. Springer Science & Business Media, 2007.
- [24] Y. H. Hu and J.-N. Hwang. *Handbook of neural network signal processing*, 2002.
- [25] D. Z. Huang, K. Xu, C. Farhat, and E. Darve. Learning constitutive relations from indirect observations using deep neural networks. *Journal of Computational Physics*, page 109491, 2020.
- [26] R. Ibañez, D. Borzacchiello, J. V. Aguado, E. Abisset-Chavanne, E. Cueto, P. Ladevèze, and F. Chinesta. Data-driven non-linear elasticity: constitutive manifold construction and problem discretization. *Computational Mechanics*, 60(5):813–826, 2017.
- [27] R. Ibanez, E. Abisset-Chavanne, J. V. Aguado, D. Gonzalez, E. Cueto, and F. Chinesta. A manifold learning approach to data-driven computational elasticity and inelasticity. *Archives of Computational Methods in Engineering*, 25(1):47–57, 2018.
- [28] S. Jung and J. Ghaboussi. Neural network constitutive model for rate-dependent materials. *Computers & Structures*, 84(15-16):955–963, 2006.

- [29] K. Karapiperis, L. Stainier, M. Ortiz, and J. Andrade. Data-driven multiscale modeling in mechanics. *Journal of the Mechanics and Physics of Solids*, page 104239, 2020.
- [30] T. Kirchdoerfer and M. Ortiz. Data-driven computational mechanics. *Computer Methods in Applied Mechanics and Engineering*, 304:81–101, 2016.
- [31] T. Kirchdoerfer and M. Ortiz. Data-driven computing in dynamics. *International Journal for Numerical Methods in Engineering*, 113(11):1697–1710, 2018. doi: 10.1002/nme.5716.
- [32] T. Kirchdoerfer and M. Ortiz. Data-driven computing in dynamics. *International Journal for Numerical Methods in Engineering*, 113(11):1697–1710, 2018.
- [33] M. Lefik and B. A. Schrefler. Artificial neural network as an incremental non-linear constitutive model for a finite element code. *Computer methods in applied mechanics and engineering*, 192(28-30):3265–3283, 2003.
- [34] M. Lefik, D. Boso, and B. Schrefler. Artificial neural networks in numerical modelling of composites. *Computer Methods in Applied Mechanics and Engineering*, 198(21-26):1785–1804, 2009.
- [35] Z. Liu and C. Wu. Exploring the 3d architectures of deep material network in data-driven multiscale mechanics. *Journal of the Mechanics and Physics of Solids*, 127:20–46, 2019.
- [36] Z. Liu, C. Wu, and M. Koishi. A deep material network for multiscale topology learning and accelerated nonlinear modeling of heterogeneous materials. *Computer Methods in Applied Mechanics and Engineering*, 345:1138–1168, 2019.
- [37] X. Lu, D. G. Giovanis, J. Yvonnet, V. Papadopoulos, F. Detrez, and J. Bai. A data-driven computational homogenization method based on neural networks for the nonlinear anisotropic electrical response of graphene/polymer nanocomposites. *Computational Mechanics*, 64(2):307–321, 2019.
- [38] F. Masi. *Fast-dynamics response and failure of masonry structures of non-standard geometry subjected to blast loads*. PhD thesis, Ecole Centrale de Nantes, 2020.
- [39] F. Masi and I. Stefanou. Thermodynamics-neural-networks. <https://github.com/flpmasi/Thermodynamics-Neural-Networks>, doi: <https://doi.org/10.5281/zenodo.4482668>, 2021.
- [40] F. Masi, I. Stefanou, P. Vannucci, and V. Maffi-Berthier. Thermodynamics-based artificial neural networks for constitutive modeling. *Journal of the Mechanics and Physics of Solids*, page 104277, 2021.
- [41] G. A. Maugin and W. Muschik. Thermodynamics with internal variables. Part I. General concepts, 1994.
- [42] M. Mozaffar, R. Bostanabad, W. Chen, K. Ehmann, J. Cao, and M. Bessa. Deep learning predicts path-dependent plasticity. *Proceedings of the National Academy of Sciences*, 116(52):26414–26420, 2019.
- [43] M. Nitka, G. Combe, C. Dascalu, and J. Desrues. Two-scale modeling of granular materials: a dem-fem approach. *Granular Matter*, 13(3):277–281, 2011.

- [44] M. Raissi, P. Perdikaris, and G. E. Karniadakis. Physics-informed neural networks: A deep learning framework for solving forward and inverse problems involving nonlinear partial differential equations. *Journal of Computational Physics*, 378:686–707, 2019.
- [45] C. Settgast, M. Abendroth, and M. Kuna. Constitutive modeling of plastic deformation behavior of open-cell foam structures using neural networks. *Mechanics of Materials*, 131:1–10, 2019.
- [46] A. Van den Eijnden, P. Bésuelle, F. Collin, R. Chambon, and J. Desrues. Modeling the strain localization around an underground gallery with a hydro-mechanical double scale model; effect of anisotropy. *Computers and Geotechnics*, 85:384–400, 2017.
- [47] K. Xu, D. Z. Huang, and E. Darve. Learning constitutive relations using symmetric positive definite neural networks. *arXiv preprint arXiv:2004.00265*, 2020.

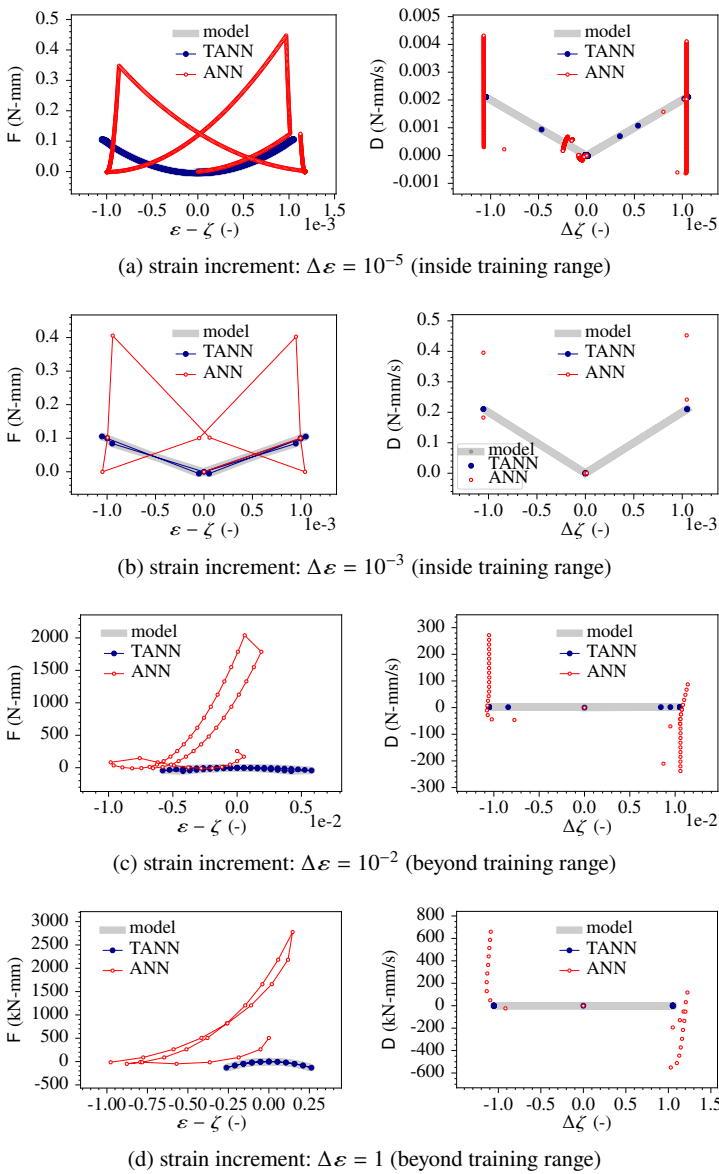
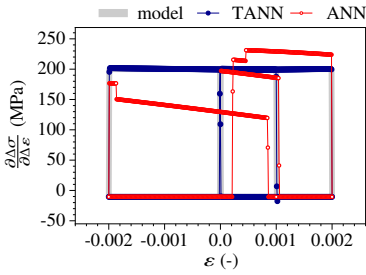
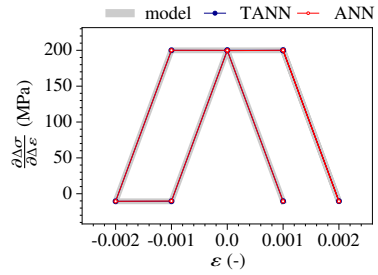


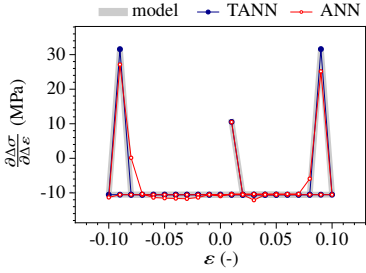
Fig. 10: Predictions of TANNs and standard ANNs for a cyclic loading path, with different strain increments (a-d), in terms of Helmholtz free energy (left column) and mechanical dissipation rate (right column).



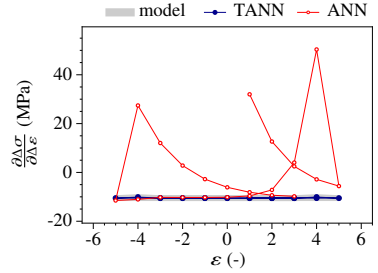
(a) strain increment: $\Delta\varepsilon = 10^{-5}$ (inside training range)



(b) strain increment: $\Delta\varepsilon = 10^{-3}$ (inside training range)



(c) strain increment: $\Delta\varepsilon = 10^{-2}$ (beyond training range)



(d) strain increment: $\Delta\varepsilon = 1$ (beyond training range)

Fig. 11: Jacobian predictions for a cyclic loading path, with different strain increments (a-d), cf. Figures 9 and 10.